# Human-Visual-System-Inspired Underwater Image Quality Measures

Karen Panetta, *Fellow, IEEE*, Chen Gao, *Student Member, IEEE*, and Sos Agaian, *Senior Member, IEEE*

*Abstract*—Underwater images suffer from blurring effects, low contrast, and grayed out colors due to the absorption and scattering effects under the water. Many image enhancement algorithms for improving the visual quality of underwater images have been developed. Unfortunately, no well-accepted objective measure exists that can evaluate the quality of underwater images similar to human perception. Predominant underwater image processing algorithms use either a subjective evaluation, which is time consuming and biased, or a generic image quality measure, which fails to consider the properties of underwater images. To address this problem, a new nonreference underwater image quality measure (UIQM) is presented in this paper. The UIQM comprises three underwater image attribute measures: the underwater image colorfulness measure (UICM), the underwater image sharpness measure (UISM), and the underwater image contrast measure (UIConM). Each attribute is selected for evaluating one aspect of the underwater image degradation, and each presented attribute measure is inspired by the properties of human visual systems (HVSs). The experimental results demonstrate that the measures effectively evaluate the underwater image quality in accordance with the human perceptions. These measures are also used on the AirAsia 8501 wreckage images to show their importance in practical applications.

*Index Terms*—AirAsia 8501 wreckage search, colorfulness measure, contrast measure, port security, sharpness measure, underwater image quality evaluation.

## I. INTRODUCTION

**T**HE quality of underwater images plays a pivotal role in ocean engineering and scientific research, such as monitoring sea life, accessing geological environment, and ocean rescue [1]. However, the absorption and scattering effects of the water limit the visibility of the underwater objects. Consequently, the images captured by underwater cameras usually suffer from low contrast, nonuniform illumination, blurring, bright artifacts, diminished color, noise, and other distortions [2].

Many algorithms have been proposed for restoring colors and enhancing contrast for observed underwater images [3]–[7]. In the majority of these methods, visual inspection is used for eval-

uating the image processing algorithms' performances. However, subjective evaluation is biased, and it is expensive with respect to time and resources. More importantly, subjective evaluation cannot be automated. Therefore, it is important to have a reliable objective evaluation measure. Generally, objective evaluation methods can be classified into two categories: nonreference measures and full-reference measures, depending on whether the images with the "true color" and "ideal contrast" are available [8]. In underwater image processing scenarios, such ideal images are usually unavailable. Therefore, the nonreference image quality measures are desired. This challenge is further exacerbated by the need to develop an underwater image quality measure that captures the objectivity and perception of the human visual system (HVS). Some generic image quality measures, such as the receiver operating characteristic (ROC) curve analysis [6], the histogram analysis [9], [10], the Michelson contrast measure [11], Hasler's colorfulness measure [12], and color image quality measure (CIQI) [13] have been developed. However, these objective measures are not designed specifically for underwater images. They fail to consider the strong absorption and scattering effects of the water and they are not able to provide a comprehensive evaluation for underwater images.

Recently, we have shown that the overall quality of an image can be effectively obtained by combinations of image attribute measures. It is natural to investigate how to tailor the image attribute measures for use in evaluating the overall underwater image quality. For underwater images, the different absorption rate for light with different wavelengths causes color casting, the forward-scattering effect generally leads to blurring of the image features, and the backward-scattering effect generally limits the contrast of the images [2]. Accordingly, the attributes of colorfulness, sharpness, and contrast, which are degraded mostly due to the property of the water media, are selected as the attributes in evaluating the overall underwater image qualities. Furthermore, it is a well-known fact that the HVS is sensitive to image structures [14] and color changes [15]. It also perceives contrast with respective to the luminance and activity changes in local regions [16]–[18]. Investigating how to tailor the HVS characteristics to each underwater image attribute measure should also be addressed.

This paper presents a new objective measure for underwater images, namely, underwater image quality measure (UIQM). The UIQM is different from commonly used HVS-based reference measures, such as mean square error (MSE) and peak signal-to-noise ratio (PSNR), which usually compute image differences between the reference and the distorted images, or measures such as structural similarity measure (SSIM) [14] and gra-

K. Panetta and C. Gao are with the Department of Electrical and Computer Engineering, Tufts University, Medford, MA 02155 USA (e-mail: Karen@ece.tufts.edu; Chen.Gao@tufts.edu).

S. Agaian is with the Department of Electrical Engineering, University of Texas at San Antonio, San Antonio, TX 78249 USA (e-mail: Sos.Agaian@utsa.edu).

dient structural similarity measure (GSSIM) [19] that attempt to quantify the difference perceptually. The UIQM does not require a reference image and it utilizes the HVS model which correlates well with the perceived underwater image quality. The remainder of this paper is organized as follows. Section II briefly presents the characteristics of HVS. Quality measures used in existing underwater image processing algorithms are also reviewed in this section. Section III presents detailed designs of the new colorfulness, sharpness, contrast measures, as well as the overall quality measure for underwater images. Section IV shows the experimental results of the presented measures for evaluating underwater image attributes and qualities. The underwater wreckage images obtained during the AirAsia 8501 blackbox retrieval are used to show the practical applications of the measures in ocean rescue. Finally, the conclusions are discussed in Section V.

## II. BACKGROUND

The goal of the new objective measures is to achieve a high correlation with human perception of image quality. To achieve this, HVS-inspired underwater image attributes measures are presented. In this section, some essential HVS phenomena that are pertinent in developing the underwater image quality measures are reviewed. Other current existing objective evaluation methods are also reviewed in this section.

### A. Human Visual System Characteristics

We choose the underwater image colorfulness, sharpness, and contrast as the basic attributes for measuring. These attributes were chosen not only for their susceptibility to change due to the physical property of the water media, such as where absorption causes color desaturation and color casting, scattering causes blurring and contrast degradations, but also because the HVS is sensitive to the changes in color, edge structures, and relative contrast [14]. That is to say, changes in these image attributes result in completely different visual appearances according to the human eye.

When quantifying the chrominance of an image, the first task is to determine which color space to use. It is observed that certain hues are never perceived to occur together such as the reddish green or the yellowish blue. According to Hering's opponent color theory, three visual quantities are opponent and paired: yellow–blue $(YB)$, red–green $(RG)$, and white–black $(WB)$. The two members of each pair are opponent, in terms of the opposite nature of the physiological processes and in terms of the mutually exclusive sensory qualities [20]. When quantifying the colorfulness property of an underwater image, the two opponent color components $RG$ and $YB$, which are related with image chrominance, should be used.

The HVS is also known to be sensitive to the relative, rather than the absolute changes in contrast [21]–[25]. The degree to which the HVS is sensitive to relative contrast varies with background illumination. Fig. 1 shows the Buchsbaum curve in which the contrast sensitivity is divided into four regions according to the background intensity [17]. Within different regions, different slopes of the contrast sensitivity are obtained. Therefore, the noticeable relative luminance differences are
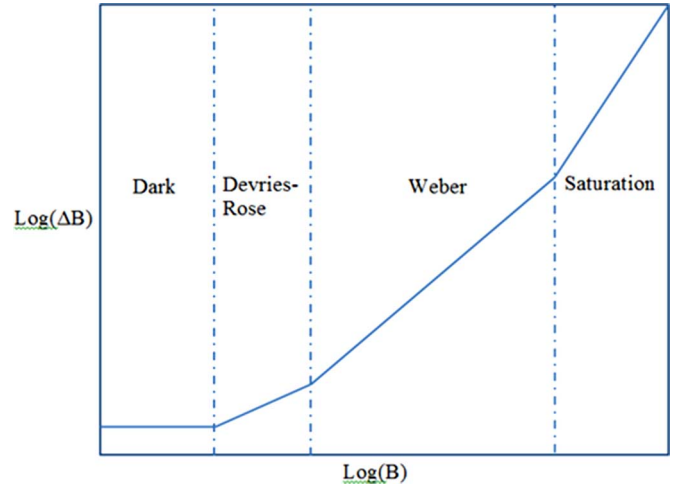


Fig. 1. Buchsbaum curve: perceived contrast $(\Delta B)$ is divided into four regions: dark region, Devries–Rose region, Weber region, and saturation region according the background intensity $(B)$.

background illumination level dependent. Accordingly, our underwater image contrast measure is formulated as a function of the relative contrast change. Edge sharpness can be seen as the contrast over the edge pixels, so a measure of the relative change is also adopted in the sharpness evaluation.

The parameterized logarithmic image processing (PLIP) provides the nonlinear representation and processing operations which are consistent with many HVS properties [26], such as brightness range inversion, Weber's Law, saturation characteristics, and context-dependent psychophysical notation [27]. The PLIP operations are also accounted for in the formulation of the underwater contrast measure.

### B. Objective Measures Used in Existing Underwater Image Processing Algorithms

Currently, objective evaluation for underwater images is still a challenge. The majority of underwater image processing algorithms results have been evaluated for their visually pleasing quality by using human observers. Some algorithms use generic image quality evaluation methods such as PSNR, MSE, and Michelson contrast to measure the enhancement performance. However, these quality measures are not designed specifically for underwater images and the application of these measures for underwater images is inadequate. Statistical analysis is used by Trucco and Olmos-Antillon [6]. To obtain the statistical values such as true positives, false positives, and equal error rate, the procedure of manually labeling the ground truth image is involved. This procedure is time consuming and cannot be automated. Hou and Weidemann proposed an objective measure based on the weighted grayscale angles (GSAs) of detected edges [28] for measuring the degree of blurring in underwater images. In their method, the gradient of the edges is used to measure the sharpness.

Histogram analysis is another type of approach used for evaluating underwater image quality. It is acknowledged that the histogram of a visually appealing image spanned over a wide range [29]. However, such histogram comparison method only results in an analytical, rather than a quantitative measure. To

overcome this limitation, some methods assume that the distribution of the gradient magnitude histogram is exponential except for a small peak at low gradient corresponding to homogeneous background [30]. Consequently, closeness of the resultant histogram to the exponential distribution is used to indicate the contrast improvement [9], [10]. The major limitation of these measures is that some important characteristics, such as colorfulness and color cast, are only accounted for indirectly.

## III. Development of the New Underwater Image Quality Measure UIQM

The new underwater image quality measure UIQM comprises three attribute measures, namely, the underwater image colorfulness measure (UICM), the underwater image sharpness measure (UISM), and the underwater image contrast measure (UIConM). Details of the new measures are presented in this section.

### A. Underwater Image Colorfulness Measure (UICM)

Many underwater images suffer from a severe color-casting problem. As the depth of the water increases, colors attenuate one by one depending on their wavelength [2]. The color red disappears first due to it possessing the shortest wavelength. As a result, underwater images usually demonstrate a bluish or greenish appearance. Furthermore, limited lighting conditions also causes severe color desaturation in underwater images. A good underwater image enhancement algorithm should produce good color rendition.

Research on natural scene colorfulness shows that colorfulness can be represented effectively with functions of image statistical values [12], [31]. Practically, users have the flexibility to choose which color spaces and which order statistical values to use, as well as the design of the fusion functions and the weighting coefficients. As mentioned before, the HVS captures colors in the opponent color plane. Therefore, the two opponent color components related with chrominance RG and YB are used in the UICM, as shown in

$$RG = R - G \tag{1}$$
$$YB = \frac{R + G}{2} - B. \tag{2}$$

Underwater images usually suffer from heavy noise. Therefore, instead of using the regular statistical values, the asymmetric alpha-trimmed statistical values [32] are used for measuring underwater image colorfulness in this paper.

For an image with size of $M$ by $N$, the total number of pixels $K = M \times N$, and all pixels of the image are sorted such that $x_1 \leq x_2 \leq \cdots \leq x_K$. Let $T_{\alpha_L} = \lceil \alpha_L K \rceil$ (the nearest integer greater than or equal to $\alpha_L K$) and $T_{\alpha_R} = \lfloor \alpha_R K \rfloor$ (the nearest integer smaller than or equal to $\alpha_R K$) be the number of the smallest and greatest pixel values to be trimmed or discarded from the sorted sequence $x_1, x_2, \ldots, x_K$. The asymmetric alpha-trimmed mean [32] is defined by

$$\mu_{\alpha,RG} = \frac{1}{K - T_{\alpha_L} - T_{\alpha_R}} \sum_{i=T_{\alpha_L}+1}^{K-T_{\alpha_R}} \text{Intensity}_{RG,i}. \tag{3}$$



$\mu_{\alpha,RG}$ = -57.2652
$\mu_{\alpha,YB}$ = -94.4343
with $\alpha_L$=0, $\alpha_R$ = 0.2
(a)

$\mu_{\alpha,RG}$ = -84.47
$\mu_{\alpha,YB}$ = -50.79
with $\alpha_L$ = $\alpha_R$ = 0
(b)

Fig. 2. (a) Underwater image with air bubbles [33]. (b) Underwater image with natural scenes [29]. In (a), the 20% brightest pixels are excluded from the calculation of the mean values because the bubbles are not related with the real scene. In (b), all pixels are considered in the calculation of the asymmetric alpha-trimmed means because this is a noise-free natural underwater scene image.



(a)                                                (b)

Fig. 3. (a) Original underwater image. (b) Color-corrected underwater image. Images courtesy of [34]. It is seen that the original image shows strong green tone, while the color-corrected image recovers more vivid color. The UICM assigns a greater measure value for the color-corrected image.

The asymmetric alpha-trimmed mean is applicable for different types of underwater images when parameters $\alpha_L$ and $\alpha_R$ change. Generally, for underwater images with lots of bubbles or light rays, such as the image in Fig. 2(a), a greater $\alpha_R$ should be used to remove the effect of the bright regions, which are not related with the natural underwater scenes, as well as some high-frequency noisy pixels, such as the salt and pepper noise. For noise-free natural scene images, such as the image in Fig. 2(b), $\alpha_L = \alpha_R = 0$ should be used. At this situation, all pixels are counted in (2) and the alpha-trimmed mean is equal to the regular mean value of the image. Similarly, the $\alpha_L$ and $\alpha_R$ portions are trimmed when calculating the high-order statistical values in (4). For the results shown in this paper, $\alpha_L = \alpha_R = 0.1$ is used.

The first-order statistic mean value $\mu$ represents chrominance intensity. A mean value that is closer to zero in the $RG$–$YB$ opponent color component implies a better white balance. That is to say, none of the colors are dominant. It is seen from Table I that the raw underwater image in Fig. 3(a) shows a strong green color and the mean value in the $RG$ color plane $\mu_{RG}$ is $-107.4312$ which implies a lot of green tone, while $\mu_{RG}$ is reduced to $-0.5760$ in the color-corrected image in Fig. 3(b). It is seen that the enhanced image in Fig. 3(b) has a more balanced color.

The second-order statistic variance $\sigma^2$ in

$$\sigma_{\alpha,RG}^2 = \frac{1}{N} \sum_{p=1}^{N} \left( \text{Intensity}_{RG,p} - \mu_{\alpha,RG} \right)^2 \tag{4}$$

TABLE I
STATISTICAL VALUES FOR IMAGES IN FIG. 3

|          | $\mu_{RG}$ | $\mu_{YB}$ | $\sigma_{RG}$ | $\sigma_{YB}$ | UICM |
|----------|-----------|-----------|--------------|--------------|--------|
| Fig. 3 (a) | -10.8300 | 61.8086 | 13.1411 | 11.0085 | -0.5889 |
| Fig. 3 (b) | 0.7896 | 0.8901 | 23.9203 | 19.9269 | 4.9058 |

demonstrates the pixel activity within each color component. Intuitively, a greater variance corresponds to a higher dynamic range. Therefore, the differences in color are more distinguishable. Table I summarizes the variances of the $RG$ and $YB$ color components for the original image in Fig. 3(a) and the color-enhanced image in Fig. 3(b). It is observed that the enhanced image in Fig. 3(b) has more vivid color, which correspond to greater variance values.

The overall colorfulness metric used for measuring underwater image colorfulness is demonstrated in

$$
\text{UICM} = -0.0268\sqrt{\mu_{\alpha,RG}^2 + \mu_{\alpha,YB}^2} \\
+ 0.1586\sqrt{\sigma_{\alpha,RG}^2 + \sigma_{\alpha,YB}^2}. \quad (5)
$$

The linear combination coefficients are obtained by linear regression. It is seen that the coefficient for the mean term is negative and the coefficient for the variance is positive, which confirm the analysis of the mathematical meaning of the two terms.

Table I shows the sensitivity of the UICM for an underwater image in Fig. 3. Fig. 3(a) suffers from severe green color casting problem. The fusion-based enhancement algorithm in [34] effectively removes the background casting as shown in Fig. 3(b). The UICM assigns a greater colorfulness measure value for the enhanced image. The results show that with image statistical values, the UICM successfully measures the colorfulness attribute for underwater images.

### B. Underwater Image Sharpness Measure (UISM)

Sharpness is the attribute related to the preservation of fine details and edges. For images captured under the water, severe blurring occurs due to the forward scattering [2]. This blurring effect causes degradation of image sharpness.

To measure the sharpness on edges, the Sobel edge detector is first applied on each RGB color component. The resultant edge map is then multiplied with the original image to get the grayscale edge map. By doing this, only the pixels on the edges from the original underwater image are preserved. It is known that the enhancement measure estimation (EME) measure is suitable for images with uniform background and shown nonperiodic patterns [35]. Accordingly, the EME measure is used to measure the sharpness of edges. The UISM is formulated as shown in

$$
\text{UISM} = \sum_{c=1}^{3} \lambda_c \text{EME} \left( \text{grayscale edge}_c \right) \quad (6)
$$

$$
\text{EME} = \frac{2}{k_1 k_2} \sum_{l=1}^{k1} \sum_{k=1}^{k_2} \log \left( \frac{I_{\max,k,l}}{I_{\min,k,l}} \right) \quad (7)
$$

where the image is divided into $k_1 k_2$ blocks, $(I_{\max,k,l})/(I_{\min,k,l})$ indicates the relative contrast ratio within each block, and the EME measures in each RGB color
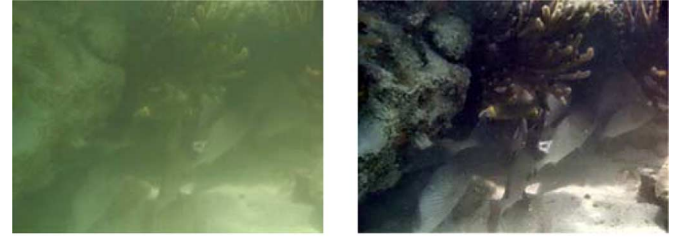


UISM = 0.5940         UISM = 3.0707
(a)            (b)

Fig. 4. (a) Original underwater image. (b) Descattered underwater image. Images courtesy of [36]. It is seen that the original image suffers from severe blurring effect, while the descattered image has sharper edges. The UISM assigns a greater measure value for the descattered image.



UIConM = 0.4732      UIConM = 1.3237
(a)            (b)

Fig. 5. (a) Original underwater image. (b) Contrast-enhanced underwater image. Images courtesy of [34]. It is seen that the original image in (a) has low contrast, while the contrast is greatly enhanced in (b). The UIConM assigns a greater measure value for the contrast-enhanced image.

component are combined linearly with coefficients $\lambda_c$, where $\lambda_R = 0.299$, $\lambda_G = 0.587$, and $\lambda_B = 0.114$ are used according to the relative visual responses of the red, green, and blue channels [30].

The descattering algorithm in [36] aims to remove the scattering effect of water. It is seen from Fig. 4 that the descattered underwater image in Fig. 4(b) achieves better sharpness than the original underwater image in Fig. 4(a). Accordingly, the descattered image in Fig. 4(b) has a greater UISM value.

### C. Underwater Image Contrast Measure (UIConM)

Contrast has been shown to correspond to underwater visual performance such as stereoscopic acuity [37]. For underwater images, contrast degradation is usually caused by backward scattering [2]. In this paper, the contrast is measured by applying the logAMEE measure [26] on the intensity image as shown in

$$
\text{UIConM} = \text{logAMEE}(\text{Intensity}). \quad (8)
$$

The logAMEE in

$$
\text{logAMEE} = \frac{1}{k_1 k_2} \otimes \sum_{l=1}^{k_1} \sum_{k=1}^{k_2} \frac{I_{\max,k,l} \Theta I_{\min,k,l}}{I_{\max,k,l} \oplus I_{\min,k,l}} \\
\times \log \left( \frac{I_{\max,k,l} \Theta I_{\min,k,l}}{I_{\max,k,l} \oplus I_{\min,k,l}} \right) \quad (9)
$$

where an image is divided into $k_1 k_2$ blocks, and $\oplus$, $\otimes$, and $\Theta$ are the PLIP operations [26], introduces the entropy-like operation to the traditional Agaian measure of enhancement by engropy (AMEE), which is formulated as the average Michaelson
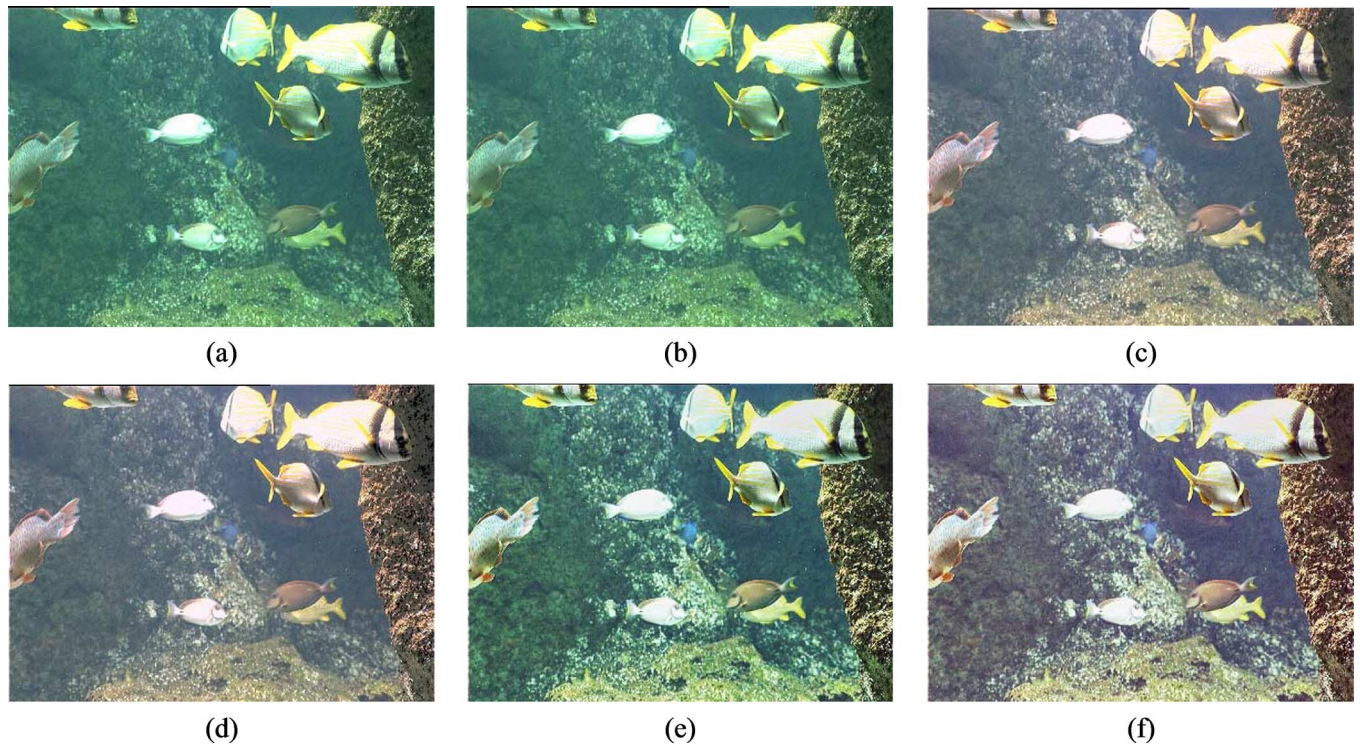
Fig. 6. (a) Original image. Color-enhanced images using (b) WP; (c) GW; (d) GWWP; and (e) ACE with original gray level preserved. (f) ACE without original gray level preserved. Images courtesy of [39].

TABLE II
COLORFULNESS MEASURE VALUES FOR IMAGES IN FIG. 6

|  | UICM | Hasler [12] | CIQI [13] |
|---|---|---|---|
| Fig. 6 (a) | 0.9657 | 13.5015 | 0.4709 |
| Fig. 6 (b) | 0.9709 | 13.5205 | 0.4711 |
| Fig. 6 (c) | 2.4832 | 7.9950 | 0.3400 |
| Fig. 6 (d) | 2.4604 | 7.9666 | 0.3337 |
| Fig. 6 (e) | 2.1758 | **14.0897** | **0.4846** |
| Fig. 6 (f) | **2.7607** | 10.2331 | 0.3484 |

TABLE III
SHARPNESS MEASURE VALUES FOR IMAGES IN FIG. 7

|  | UISM | CIQI_sharpness [40] |
|---|---|---|
| Fig. 7 (b) | 2.4162 | 0.3588 |
| Fig. 7 (c) | **5.0368** | 0.3740 |
| Fig. 7 (d) | 2.4117 | 0.3167 |
| Fig. 7 (e) | 2.4846 | 0.3378 |
| Fig. 7 (f) | 2.3870 | **0.4688** |

contrast in image local regions. The PLIP operations, which provides the nonlinear representations that are consistent with human visual perceptions [26], are also used in the logAMEE formulation. Practically, lighting conditions are usually poor under the water. In such cases, the logAMEE is preferred for the reason that the log and PLIP operations [26] put more emphasis on areas with low luminance [35].

Fig. 5 shows an example of applying a contrast enhancement algorithm [34] on an underwater image in Fig. 5(a). It is observed that the visibility is greatly improved in Fig. 5(b). The UIConM also assigns a greater value for the enhanced image.

### D. Underwater Image Quality Measure (UIQM)

It has been demonstrated that underwater images can be modeled as linear superposition of absorbed and scattered components [38]. Besides, it is known that the absorption and scattering effects cause color, sharpness, and contrast degradation. Therefore, it is reasonable to use the linear superposition model for generating the overall underwater image quality measure as well. The overall underwater image quality measure is then given by

$$\text{UIQM} = c_1 \times \text{UICM} + c_2 \times \text{UISM} + c_3 \times \text{UIConM} \quad (10)$$

where the colorfulness, sharpness, and contrast measures are linearly combined together. It is worth noting that the UIQM in (10) has three parameters $c_1$, $c_2$, and $c_3$. The selections of these parameters are application dependent. For example, for underwater image color-correction applications, more weights should be applied to the UICM, while in enhancing underwater image visibilities, the contrast term UIConM and the sharpness term UISM are more significant. If two of the parameters are zero, the quality measure UIQM reverts to an underwater image attribute measure. For general applications, the combination coefficients are obtained using multiple linear regression (MLR). The training data set shown in this paper contains 30 randomly selected underwater images captured with variant devices and under variant depths of the water. For the results shown in this paper, a generic coefficient set $c_1 = 0.0282$, $c_2 = 0.2953$, and $c_3 = 3.5753$ is used. The overall model is significant with a $P$-value equal 0.0339. The measures can be used to evaluate the performances of image enhancement algorithms. Generally, a greater UIQM value corresponds to an image with a better
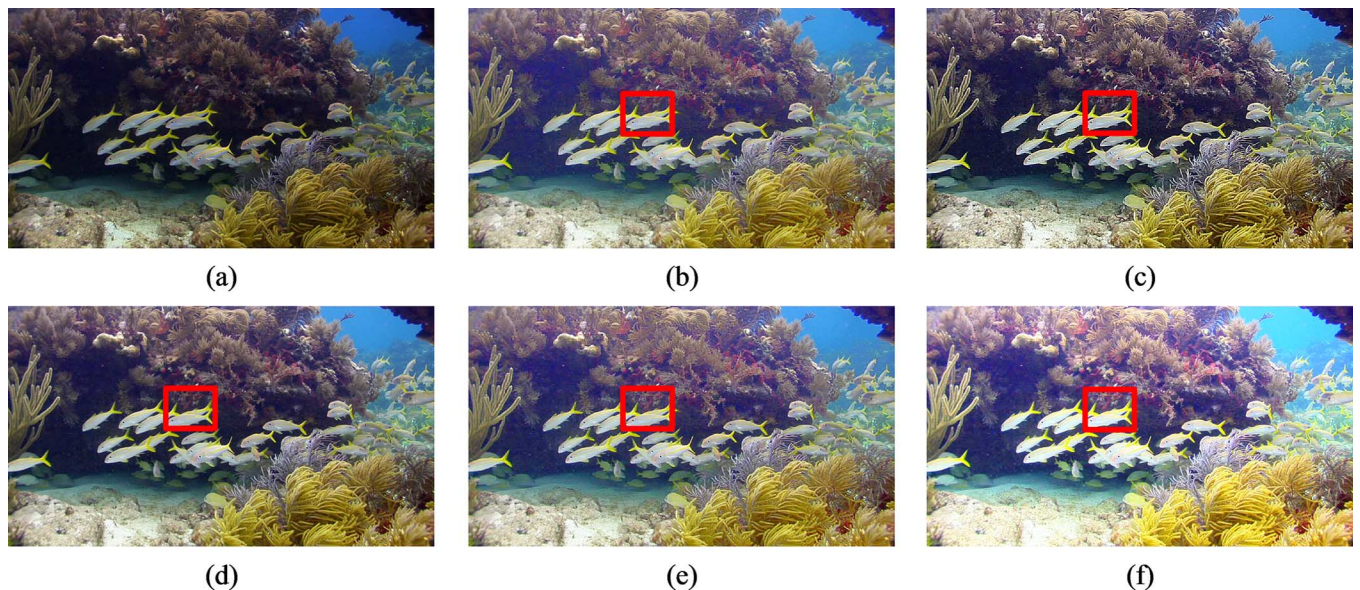
Fig. 7.  (a) Original image. Enhancement results from (b) DRC_CES; (c) MCE; (d) MCE_DRC; (e) SF_CES; and (f) TW_CES. The original image is obtained from the SUN database [44].
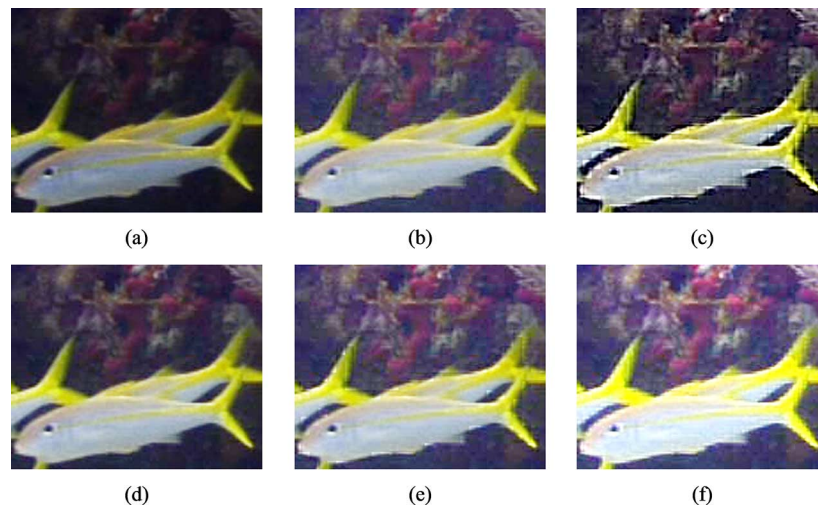


Fig. 8.  Zoomed in view of the region of interest for the images from Fig. 7. (a) Original image. Enhancement results from (b) DRC_CES; (c) MCE; (d) MCE_DRC; (e) SF_CES; and (f) TW_CES.

quality, and a 10% increase in terms of the UIQM measure value leads to a visually distinguishable improvement.

## IV. Experimental Results

The underwater image quality measure UIQM can be used for evaluating the overall underwater image quality in a similar manner as human observers. Each attribute measure can also be used as a standalone measure for specific underwater image processing tasks. In this section, the presented underwater attribute measures and quality measure are used to benchmark image processing algorithms' performances, as well as to assist in the selection of optimal operating parameters. Comparisons with existing image attribute measures and overall quality measures are also demonstrated.

Fig. 6(a) shows an underwater image with different fish species (the original image and the processed images by Chambah *et al.* [39]). The original image suffers from poor color dynamic range and strong cyan-green cast. Fig. 6(b)–(f) demonstrates enhanced images from different algorithms. The

TABLE IV
CONTRAST MEASURE VALUES FOR IMAGES IN FIG. 9

|            | UIConM | CIQI_contrast | CRME   | SDME   |
|------------|--------|---------------|--------|--------|
| Fig. 9 (b) | 1.1456 | 0.1419        | 0.7970 | 0.9928 |
| Fig. 9 (c) | **1.2841** | 0.2289    | **0.9018** | **1.9778** |
| Fig. 9 (d) | 1.1377 | 0.1374        | 0.7512 | 1.4656 |
| Fig. 9 (e) | 1.1597 | 0.1861        | 0.8024 | 0.9957 |
| Fig. 9 (f) | 1.1732 | **0.2818**    | 0.8332 | 0.9778 |

TABLE V
PERFORMANCE COMPARISONS OF THE QUALITY MEASURES FOR UNDERWATER
IMAGES. THE UIQM HAS GREATER PEARSON, SPEARMAN, AND KENDALL
CORRELATIONS FOR THESE UNDERWATER IMAGES
OBTAINED FROM THE SUN DATABASE

|       | SRCC   | PRCC   | KRCC   |
|-------|--------|--------|--------|
| CRME  | 0.2845 | 0.5712 | 0.2576 |
| CIQI  | 0.2941 | 0.2848 | 0.2495 |
| JPQM  | 0.5063 | 0.6113 | 0.3944 |
| UIQM  | **0.5571** | **0.6582** | **0.5071** |

Fig. 9. (a) Original image. Enhancement results from (b) DRC_CES; (c) DRC_CES_BLK; (d) MCE_DRC; (e) SF_CES; and (f) TW_CES. The original image is obtained from the SUN database [44].



Fig. 10. The fourteen images used to test the performances of the quality measures.

UICM, Hasler's color measure [12], and the CIQI colorfulness measure [13] values are listed in Table II. Comparing these images, it can be seen that the white patch (WP) method [39] [Fig. 6(b)] does not change the original image much, since the original image is oversaturated. Accordingly, the UICMs for these two images are similar [0.9657 for Fig. 6(a) and 0.9709 for Fig. 6(b)]. The gray world (GW) method [39] [Fig. 6(c)] produces an overall color-balanced image, but the obtained image shows slight reddish cast. It is seen that the UICM increases almost 1.5 times. The gray world white patch (GWWP) hybrid method [39] [Fig. 6(d)] has similar performance as GW since the WP has little effect on the image. Accordingly, the UICM values for Fig. 6(c) and (d) are comparable. The automatic color equalization (ACE) method with original gray level preserved [Fig. 6(e)] achieves a better dynamic range, but it still suffers from some background color casting. The best result is obtained with the ACE method without the "keep original gray" feature [Fig. 6(f)]. Using this algorithm, the color cast is removed and the resultant image is chromatically diverse. The UICM conforms to the analyses in [39] and denotes that the ACE method without the "keep original gray" feature has the optimal performance. The Hasler's colorfulness measure for general natural images [12] and the CIQI colorfulness

measure [13] are used for comparison purposes. Contrarily, these two methods select the "ACE method with the original gray preserved" [Fig. 6(e)] as the optimal image without taking the green color cast into consideration.

We then compare the performances of the sharpness measures and the contrast measures. Two examples are shown in Figs. 7 and 9. The images in Figs. 7(a) and 9(a) suffer from blurring effects. The intensities of the images are first adjusted using the modified Naka–Rushton function [40]. Then, contrast enhancement algorithms are applied including multicontrast enhancement (MCE) [41]; multicontrast enhancement with dynamic range compression (MCEDRC) [42]; and contrast enhancement by scaling (CES) using twicing-function (TW_CES), S-function (SF_CES), and dynamic range compression (DRC_CES) [41], [43]. Note that the original images obtained from the Scene Understanding (SUN) database [44] are JPEG compressed images. Some of the image enhancement algorithms enhance the block artifacts as well. To exclude the effects of the JPEG blocks, the size of the local region $k_1k_2$ used in (7) and (9) is selected as $8 \times 8$ when calculating the UISM and the UIConM.

Table III shows the comparisons of the UISM with CIQI sharpness. It is seen that the MCE result in Fig. 7(c) is the
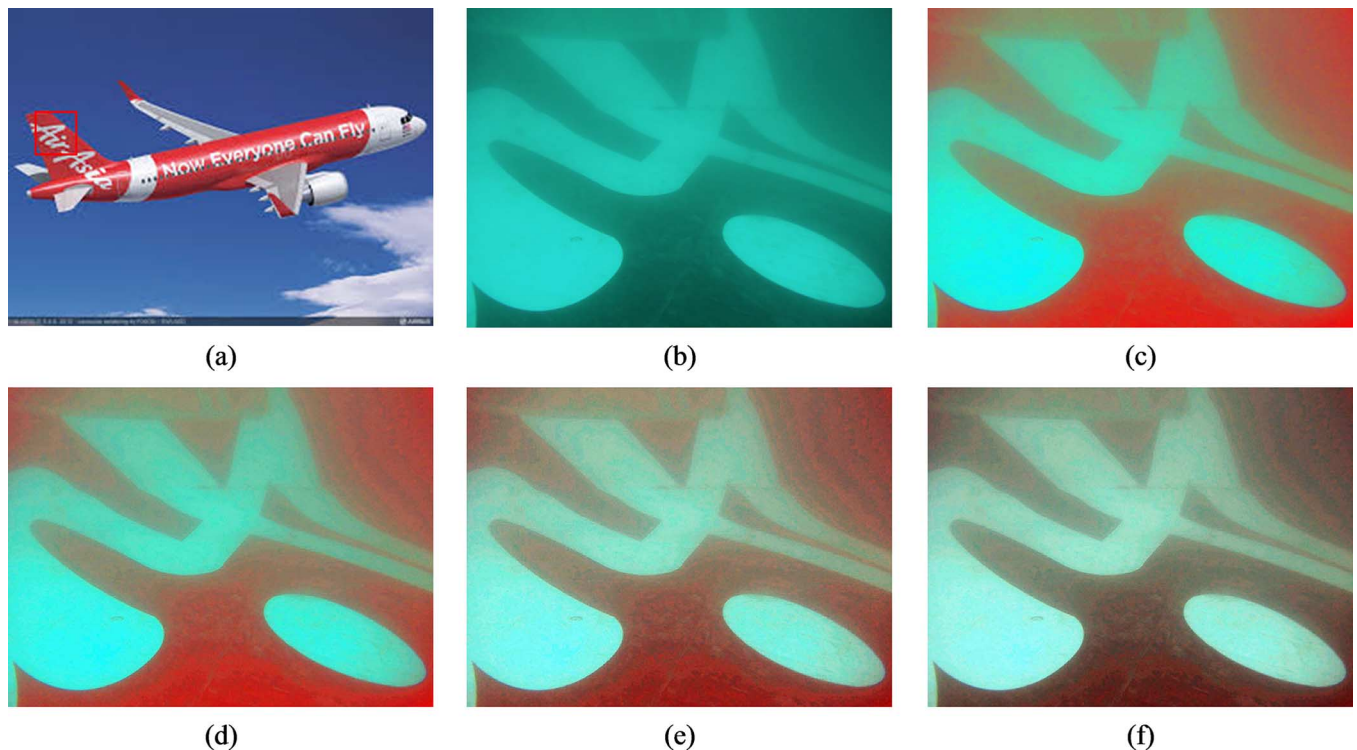
Fig. 11. (a) AirAsia plane. (b) Image from the wreckage of the AirAsia 8501 plane's tail found underwater. (c)–(f) Color-enhancement results using the 3DAWQF with parameter $M$ equal to 12, 20, 28, and 36, respectively.

TABLE VI
ATTRIBUTE AND QUALITY MEASURES FOR THE IMAGES IN FIG. 13. THE OPTIMAL RESULTS CORRESPONDING TO EACH MEASURE ARE HIGHLIGHTED IN BOLD, AND THE WORST RESULTS ARE HIGHLIGHTED IN ITALIC AND UNDERSCORE

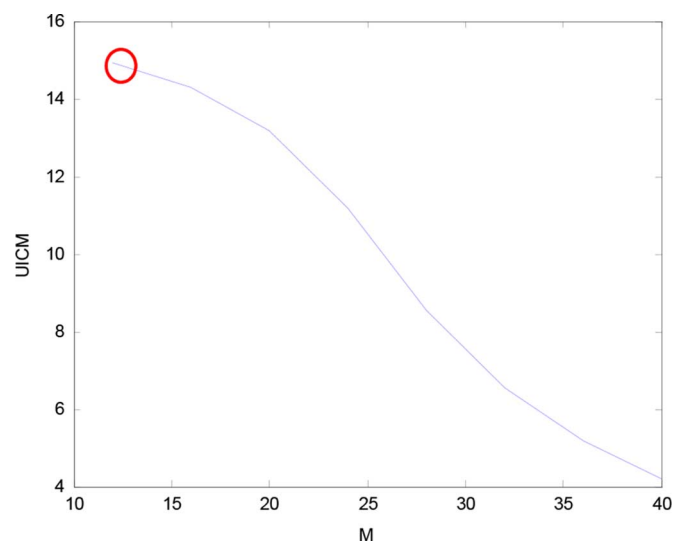| | UICM | UISM | UIConM | UIQM |
|---|---|---|---|---|
| Fig. 10 (c) | 9.4518 | 0.6242 | 0.4259 | 0.5062 |
| Fig. 10 (d) | 6.7425 | **1.0281** | **0.5666** | **0.6462** |
| Fig. 10 (e) | 6.7983 | 0.6217 | 0.4243 | 0.4854 |
| Fig. 10 (f) | 6.6958 | 0.7221 | 0.4722 | 0.5361 |
| Fig. 10 (g) | 4.9047 | _0.5995_ | _0.3598_ | _0.4108_ |
| Fig. 10 (h) | _2.7972_ | 0.8176 | 0.4910 | 0.5324 |
| Fig. 10 (i) | **6.9774** | 0.8682 | 0.4785 | 0.5551 |



Fig. 12. UICM values for varying parameter $M$ in the 3DAWQF filter design. In 3DAWQF, $M$ is used to control the influence of neighboring pixels to the center pixel of the color cube in the algorithm. It is seen that the UICM achieves the greatest value at $M = 12$, which corresponds to the enhanced image with the best color quality in Fig. 11(c).

sharpest in terms that the edges of all the fish and the corals are more distinctive. Correspondingly, the UISM accurately selects the MCE result as the one with the optimal sharpness. Although the TW_CES result in Fig. 7(f) also has sharp visual appearances on the dark portion of the image, it is oversaturated on the bright portion of the image. Therefore, some details are not visible such as the stripes on the fish. The regions of interest in the red rectangles are shown in Fig. 8. Similarly, an illustrative example of using the UIConM, CIQI contrast measure, cube root mean enhancement (CRME) [40], and second derivative-like measure of enhancement (SDME) [45] for evaluating the underwater image contrast quality is shown in Fig. 9, and the measure values are demonstrated in Table IV. The experimental results show that the presented measures have strong correlation with the subjective perception.

Fourteen images are randomly selected from the SUN database [44] and used to test the correlations of the image quality measures with subjective evaluations. These 14 images, shown

in Fig. 10, include corals, divers, fish, rocks, ice, wreckages, and other underwater scenes captured from variant depths of ocean. Nine enhancement results for each image are generated [43] and used to compare the correlations between the objective measure values and the mean opinion scores (MOS) gathered from ten experts of image processing area. Three correlations are used: Pearson's linear product moment correlation (PRCC), which measures how far each measure value deviates from the MOS [46]; Spearman's rank order correlation (SRCC), which
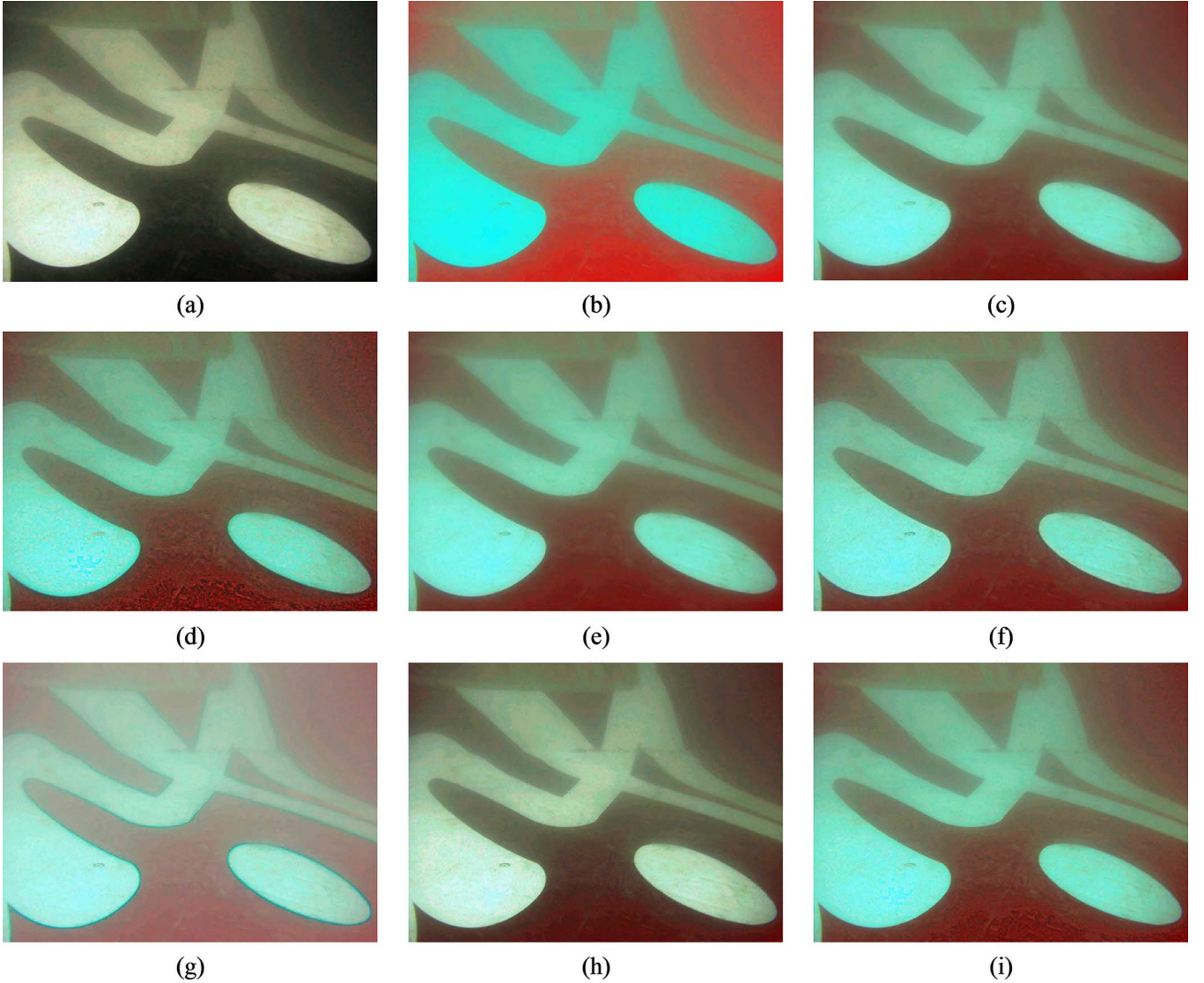
Fig. 13. Using presented underwater image attribute measures and underwater quality measures to select the optimal fusion method used in the 3DAWQF image-enhancement algorithm. (a) Intensity-corrected and contrast-enhanced image. (b) Color-enhanced image. (c) Filter-subtract-decimate pyramid fusion. (d) Contrast pyramid fusion. (e) Gradient pyramid fusion. (f) Laplacian pyramid fusion. (g) Morphological difference pyramid fusion. (h) PLIP fusion. (i) Ratio pyramid fusion.

compares the rank of image qualities; and Kendall's tau correlation (KRCC), which is usually suggested for measuring rank of nonnormal data [47]. The three indexes are defined as

$$\text{Pearson}(a, b)$$
$$= \frac{\sum_{k=1}^{K}(a_k - \bar{a})(b_k - \bar{b})}{\sqrt{\sum_{k=1}^{K}(a_k - \bar{a})^2}\sqrt{\sum_{k=1}^{K}(b_k - \bar{b})^2}} \qquad (11)$$

$$\text{Spearman}(a, b)$$
$$= \frac{\sum_{k=1}^{K}(R(a_k) - \overline{R(a)})(R(b_k) - \overline{R(b)})}{\sqrt{\sum_{k=1}^{K}(R(a_k) - \overline{R(a)})^2}\sqrt{\sum_{k=1}^{K}(R(b_k) - \overline{R(b)})^2}}$$
$$(12)$$

$$\text{Kendall}(a, b)$$
$$= \frac{N(\text{concordant pairs}) - N(\text{discordant pairs})}{\frac{1}{2}K(K-1)} \qquad (13)$$

where $a$ and $b$ represent two variables, $\bar{a}$ and $\bar{b}$ are the mean values of $a$ and $b$, $R$ represents the rank, and $N$ represents the

total number of variables. The average correlation coefficients for these 14 images are tabulated in Table V. It is seen that the UIQM has the greatest SRCC, PRCC, and KRCC values compared to CIQI [13], CRME [40], and JPQM [48].

Practically, the measures are also important in the design of underwater image processing algorithms, which can be used in monitoring sea life, accessing geological and biological environment information, as well as port security inspection. The low visibility and strong color casting bring difficulties for the underwater searching and inspection. Therefore, image contrast and color enhancement algorithms are usually used to enhance the vision of underwater vehicles or robots. In the following examples, the three-dimensional alpha weighted quadratic filter (3DAWQF) [40] is used to enhance the contrast and the colors, and the measures are used to assist in the selection of the optimal operating parameters used in the 3DAWQF.

One example of the practical applications of the underwater image attribute and quality measures is to assist in underwater search. Fig. 11(b) shows one image captured by a remotely op-

erated underwater vehicle during the retrieval of the blackbox from the AirAsia 8501 disaster. It is seen that the real color of the plane's tail [Fig. 11(a)] is not recognizable from the captured underwater image because the image shows a strong blue casting. In the 3DAWQF algorithm, a highpass filter is applied across the RGB color planes to recover colors. In the highpass filter used in 3DAWQF, a parameter $M$ is used to control the influence of neighboring pixels to the center pixel of the color cube [40]. Fig. 11(c)–(f) shows color enhancement results with variant parameter $M$. It is seen that more color information is restored with a smaller value of $M$. A greater value of $M$ also introduces some artifacts. The values of the UICM for parameter $M$ ranging from 12 to 40 (Fig. 12) confirm the visual observations that a smaller $M$ corresponds to a better color quality. Therefore, a parameter $M$ equal to 12 is used in the 3DAWQF design.

Similarly, the UIConM can be used to assist the selection of optimal operating parameters used in the 3DAWQF contrast enhancement. After the optimal contrast-enhanced image [Fig. 13(a)] and the color-enhanced image [Fig. 13(b)] are obtained, these two images are fused together to generate the final output. Multiple fusion methods can be used [49], and fusion results from the filter-subtract-decimate pyramid, the contrast pyramid, the gradient pyramid, the Laplacian pyramid, the morphological difference pyramid, the PLIP addition [26], and the ratio pyramid are shown in Fig. 13(e)–(i). The measure values for these fused images are tabulated in Table IV. From these measures, it is seen that the ratio pyramid fusion [Fig. 13(i)] has the most vivid color, while the PLIP fusion [Fig. 13(h)] has the least vivid color. The contrast pyramid fusion [Fig. 13(d)] has the best contrast, while the morphological difference pyramid fusion [Fig. 13(g)] has the worst contrast. The overall quality from the contrast pyramid fusion [Fig. 13(d)] is the best. These measures conform to the human perceptions. It is worth noting that for flight wreckage searching applications, similar aircraft models have similar painting colors. Therefore, the real painting colors are used in this section to validate the performance of the UICM. In many other applications such as underwater geological and biology inspection, such reference images are not available. The nonreference measures presented in this paper are able to serve these applications as well.

## V. Conclusion

In this paper, a new nonreference underwater image quality measure UIQM was presented. The UIQM comprises a colorfuless measure (UICM), a sharpness measure (UISM), and a contrast measure (UIConM). Each attribute measure can be used separately for specific underwater image processing tasks. Several HVS properties, such as luminance and contrast masking, the color perception property, and relative contrast sensitivity, are incorporated in the formulations of the measures. Therefore, comparing with other quality measures used in existing underwater image processing algorithms, the UIQM has stronger correlation with human visual perception, and it effectively measures the underwater image quality in a complete and comprehensive means. The measures were applied to evaluating images of the AirAsia 8501 wreckage. The results demonstrated that the attribute measures UICM, UISM, and UIConM, as well as the

underwater image quality measure UIQM can be effective tools to assist in selecting optimal operating parameters used in underwater enhancement algorithms as well as to rank algorithms' performances.

## References

[1] J. Y. Chiang and Y.-C. Chen, "Underwater image enhancement by wavelength compensation and dehazing," *IEEE Trans. Image Process.*, vol. 21, no. 4, pp. 1756–1769, Apr. 2012.

[2] S. Raimondo and C. Silvia, "Underwater image processing: State of the art of restoration and image enhancement methods," *EURASIP J. Adv. Signal Process.*, vol. 2010, 2010, DOI: 10.1155/2010/746052.

[3] W. Hou, D. J. Gray, A. D. Weidemann, G. R. Fournier, and J. Forand, "Automated underwater image restoration and retrieval of related optical properties," in *Proc. IEEE Int. Geosci. Remote Sens. Symp.*, 2007, pp. 1889–1892.

[4] Z. Liu, Y. Yu, K. Zhang, and H. Huang, "Underwater image transmission and blurred image restoration," *Opt. Eng.*, vol. 40, pp. 1125–1131, 2001.

[5] J. Åhlén, D. Sundgren, and E. Bengtsson, "Application of underwater hyperspectral data for color correction purposes," *Pattern Recognit. Image Anal.*, vol. 17, pp. 170–173, 2007.

[6] E. Trucco and A. T. Olmos-Antillon, "Self-tuning underwater image restoration," *IEEE J. Ocean. Eng.*, vol. 31, no. 2, pp. 511–519, Apr. 2006.

[7] B. Ouyang *et al.*, "Visualization and image enhancement for multistatic underwater laser line scan system using image-based rendering," *IEEE J. Ocean. Eng.*, vol. 38, no. 3, pp. 566–580, Jul. 2013.

[8] C. Gao, K. Panetta, and S. Agaian, "Color image retrieval and analysis using image color measures," *Proc. SPIE—Sens. Technol. Appl.*, vol. 9497, 2015, DOI: 10.1117/12.2180605.

[9] S. Bazeille, I. Quidu, L. Jaulin, and J.-P. Malkasse, "Automatic underwater image pre-processing," in *Proc. Caracterisation Du Milieu Marin*, 2006.

[10] A. Arnold-Bos, J.-P. Malkasse, and G. Kervern, "Towards a model-free denoising of underwater optical images," in *Proc. IEEE OCEANS Conf.*, 2005, pp. 527–532.

[11] Y. Y. Schechner and N. Karpel, "Recovery of underwater visibility and structure by polarization analysis," *IEEE J. Ocean. Eng.*, vol. 30, no. 3, pp. 570–587, Jul. 2005.

[12] D. Hasler and S. E. Susstrunk, "Measuring colorfulness in natural images," *Proc. SPIE—Int. Soc. Opt. Eng.*, vol. 5007, pp. 87–95, 2003.

[13] Y.-Y. Fu, "Color image quality measures and retrieval," Ph.D. dissertation, Dept. Comput. Sci., New Jersey Inst. Technol., Hoboken, NJ, USA, 2006.

[14] Z. Wang, A. C. Bovik, H. R. Sheikh, and E. P. Simoncelli, "Image quality assessment: From error visibility to structural similarity," *IEEE Trans. Image Process.*, vol. 13, no. 4, pp. 600–612, Apr. 2004.

[15] M. Sarifuddin and R. Missaoui, "A new perceptually uniform color space with associated color similarity measure for content-based image and video retrieval," in *Proc. ACM SIGIR Workshop Multimedia Inf. Retrieval*, 2005, pp. 1–8.

[16] S. G. Mallat, "A theory for multiresolution signal decomposition: The wavelet representation," *IEEE Trans. Pattern Anal. Mach. Intell.*, vol. 11, no. 7, pp. 674–693, Jul. 1989.

[17] G. Buchsbaum, "An analytical derivation of visual nonlinearity," *IEEE Trans. Biomed. Eng.*, vol. BME-27, no. 5, pp. 237–242, May 1980.

[18] G. E. Legge and J. M. Foley, "Contrast masking in human vision," *J. Opt. Soc. Amer.*, vol. 70, pp. 1458–1471, 1980.

[19] S. Nercessian, S. S. Agaian, and K. A. Panetta, "An image similarity measure using enhanced human visual system characteristics," *Proc. SPIE—Int. Soc. Opt. Eng.*, vol. 8063, 2011, DOI: 10.1117/12.883301.

[20] L. M. Hurvich and D. Jameson, "An opponent-process theory of color vision," *Psychol. Rev.*, vol. 64, p. 384, 1957.

[21] K. A. Panetta, E. J. Wharton, and S. S. Agaian, "Human visual system-based image enhancement and logarithmic contrast measure," *IEEE Trans. Syst. Man Cybern. B, Cybern.*, vol. 38, no. 1, pp. 174–188, Feb. 2008.

[22] E. Wharton, S. Agaian, and K. Panetta, "A logarithmic measure of image enhancement," in *Proc. Defense Security Symp.*, 2006, pp. 62500P–62500P-12.

[23] S. S. Agaian, K. Panetta, and A. M. Grigoryan, "A new measure of image enhancement," in *Proc. IASTED Int. Conf. Signal Process. Commun.*, 2000, pp. 19–22.

[24] S. S. Agaian, B. Silver, and K. A. Panetta, "Transform coefficient histogram-based image enhancement algorithms using contrast entropy," *IEEE Trans. Image Process.*, vol. 16, no. 3, pp. 741–758, Mar. 2007.

[25] S. S. Agaian, "Visual morphology," *Proc. SPIE—Int. Soc. Opt. Eng.*, vol. 3646, pp. 139–150, 1999.

[26] K. Panetta, S. Agaian, Y. Zhou, and E. J. Wharton, "Parameterized logarithmic framework for image enhancement," *IEEE Trans. Syst. Man Cybern. B, Cybern.*, vol. 41, no. 2, pp. 460–473, Apr. 2011.

[27] G. Deng, L. Cahill, and G. Tobin, "The study of logarithmic image processing model and its application to image enhancement," *IEEE Trans. Image Process.*, vol. 4, no. 4, pp. 506–512, Apr. 1994.

[28] W. Hou and A. D. Weidemann, "Objectively assessing underwater image quality for the purpose of automated restoration," in *Proc. Defense Security Symp.*, 2007, pp. 65750Q–65750Q-7.

[29] K. Iqbal, R. A. Salam, M. Osman, and A. Z. Talib, "Underwater image enhancement using an integrated colour model," *IAENG Int. J. Comput. Sci.*, vol. 32, pp. 239–244, 2007.

[30] , W. K. Pratt, Ed., *Digital Image Processing*. New York, NY, USA: Wiley, 1991, ch. 2.

[31] C. Gao, K. Panetta, and S. Agaian, "No reference color image quality measures," in *Proc. IEEE Int. Conf. Cybern.*, 2013, pp. 243–248.

[32] J. Bednar and T. L. Watt, "Alpha-trimmed means and their relationship to median filters," *IEEE Trans. Acoust. Speech Signal Process.*, vol. ASSP-32, no. 1, pp. 145–153, Feb. 1984.

[33] Eagle Point Resort, "Scuba diving—Bubble mechanics," Sep. 5, 2014 [Online]. Available: http://eaglepointresort.com.ph/scuba-diving-bubble-mechanics/

[34] C. Ancuti, C. O. Ancuti, T. Haber, and P. Bekaert, "Enhancing underwater images and videos by fusion," in *Proc. IEEE Conf. Comput. Vis. Pattern Recognit.*, 2012, pp. 81–88.

[35] K. Panetta, A. Samani, and S. Agaian, "Choosing the optimal spatial domain measure of enhancement for mammogram images," *J. Biomed. Imag.*, 2014, Article ID 937849.

[36] T. Treibitz and Y. Y. Schechner, "Active polarization descattering," *IEEE Trans. Pattern Anal. Mach. Intell.*, vol. 31, no. 3, pp. 385–399, Mar. 2009.

[37] S. Luria and J. A. S. Kinney, "Underwater vision," *Amer. Assoc. Adv. Sci.*, vol. 167, pp. 1454–1461, 1970.

[38] L. Mertens and F. Replogle, Jr., "Use of point spread and beam spread functions for analysis of imaging systems in water," *J. Opt. Soc. Amer.*, vol. 67, pp. 1105–1117, 1977.

[39] M. Chambah, D. Semani, A. Renouf, P. Courtellemont, and A. Rizzi, "Underwater color constancy: Enhancement of automatic live fish recognition," *Proc. SPIE—Int. Soc. Opt. Eng.*, pp. 157–168, 2003, DOI: 10.1117/12.524540.

[40] C. Gao, K. Panetta, and S. Agaian, "Three dimensional alpha weighted quadratic filter based image color contrast enhancement," *Proc. SPIE—Int. Soc. Opt. Eng.*, vol. 8755, 2013, DOI:10.1117/12.2015619.

[41] J. Tang, E. Peli, and S. Acton, "Image enhancement using a contrast measure in the compressed domain," *IEEE Signal Process. Lett.*, vol. 10, no. 10, pp. 289–292, Oct. 2003.

[42] S. Lee, "An efficient content-based image enhancement in the compressed domain using retinex theory," *IEEE Trans. Circuits Syst. Video Technol.*, vol. 17, no. 2, pp. 199–213, Feb. 2007.

[43] J. Mukherjee and S. K. Mitra, "Enhancement of color images by scaling the DCT coefficients," *IEEE Trans. Image Process.*, vol. 17, no. 10, pp. 1783–1794, Oct. 2008.

[44] J. Xiao, J. Hays, K. Ehinger, A. Oliva, and A. Torralba, "Sun database: Large-scale scene recognition from abbey to zoo," in *Proc. IEEE Conf. Comput. Vis. Pattern Recognit.*, 2010, pp. 3485–3492.

[45] K. Panetta, Y. Zhou, S. Agaian, and H. Jia, "Nonlinear unsharp masking for mammogram enhancement," *IEEE Trans. Inf. Technol. Biomed.*, vol. 15, no. 6, pp. 918–928, Nov. 2011.

[46] I. Lawrence and K. Lin, "A concordance correlation coefficient to evaluate reproducibility," *Biometrics*, vol. 45, pp. 255–268, 1989.

[47] J. B. Carroll, "The nature of the data, or how to choose a correlation coefficient," *Psychometrika*, vol. 26, pp. 347–372, 1961.

[48] Z. Wang, H. R. Sheikh, and A. C. Bovik, "No-reference perceptual quality assessment of JPEG compressed images," in *Proc. IEEE Int. Conf. Image Process.*, 2002, vol. 1, pp. 477–480.

[49] Fusion Toolbox [Online]. Available: http://www.metapix.de/fusion.htm

**Karen Panetta** (S'84–M'85–SM'95–F'08) received the B.S. degree in computer engineering from Boston University, Boston, MA, USA and the M.S. and Ph.D. degrees in electrical engineering from Northeastern University, Boston, MA, USA, in 1994.

She is currently an Associate Dean of Graduate Engineering Education and a Professor in the Department of Electrical and Computer Engineering, Tufts University, Medford, MA, USA, and Director of the Simulation Research Laboratory. Her research focuses on developing efficient algorithms for simulation, modeling, signal, and image processing for biomedical and security applications.

Dr. Panetta is the Editor-in-Chief of the IEEE WOMEN IN ENGINEERING magazine. She is the IEEE-USA Vice-President of Communications and Public Affairs. She also served as the 2011 Chair of the IEEE Boston Section, which has over 8800 members. During 2007–2009, she served as the world wide Director for IEEE Women in Engineering, overseeing the world's largest professional organization supporting women in engineering and science. She is also the recipient of the 2012 IEEE Ethical Practices Award and the Harriet B. Rigas Award for Outstanding Educator. In 2011, she was awarded the Presidential Award for Engineering and Science Education and Mentoring by U.S. President Barack Obama.
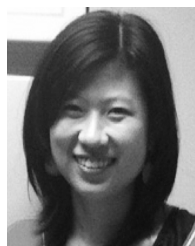
**Chen Gao** (S'10) received the B.S. degree in electrical engineering from Beijing Normal University, Beijing, China, in 2008 and the M.S. degree in electrical and computer engineering from Polytechnic Institute of New York University, Brooklyn, NY, USA, in 2010. Currently, she is working toward the Ph.D. degree in image processing at Tufts University, Medford, MA, USA.

Her research interests include image contrast enhancement, color enhancement, edge detection, and image quality assessment.

Miss Gao is a student member of Women in Engineering (WIE) and the International Society for Optics and Photonics (SPIE).

**Sos Agaian** (M'98–SM'00) received the M.S. degree (*summa cum laude*) in mathematics and mechanics from Yerevan University, Yerevan, Armenia, the Ph.D. degree in math and physics from the Steklov Institute of Mathematics, Russian Academy of Sciences, Moscow, Russia, and the Doctor of Engineering Sciences degree from the Institute of the Control System, Russian Academy of Sciences, Moscow, Russia, in 1988.

He is Peter T. Flawn Professor of Electrical and Computer Engineering at the University of Texas San Antonio, San Antonio, TX, USA, and Professor at the University of Texas Health Science Center, San Antonio, TX, USA. He has authored more than 550 scientific papers and seven books, and holds 18 patents. His research interests are multimedia processing, imaging systems, information security, artificial intelligent, computer vision, 3-D imaging sensors, signal and information processing in finance and economics, and biomedical and health informatics.

Dr. Agaian is a Fellow of the International Society for Photo-Optical Instrumentations Engineers, the Society for Imaging Science and Technology (IS&T), and the Science Serving Society (AAAS). He also serves as a foreign member of the Armenian National Academy. He is the recipient of MAEStro Educator of the Year, sponsored by the Society of Mexican American Engineers and Scientists. The technologies he invented have been adopted across multiple disciplines, including the U.S. Government, and commercialized by industry. He is an Editorial Board Member of the *Journal of Pattern Recognition and Image Analysis* and an Associate Editor for several journals, including the *Journal of Electronic Imaging* (SPIE, IS&T) and the IEEE SYSTEM JOURNAL.